

Study of Structural Phase Transformations in the Metal of Welded Joints of Reactor Plants for Nuclear Icebreakers

M. N. Timofeev^a, R. I. Samoylenko^{a,*}, S. N. Galyatkin^a, Yu. M. Markova^a,
D. M. Anisimov^a, S. A. Korolev^b, and S. V. Gurkin^b

^a National Research Center Kurchatov Institute—Central Research Institute of Structural Materials Prometey, St. Petersburg, 191015 Russia

^b Bauman Moscow State Technical University, Moscow, 105005 Russia

*e-mail: roma.samoylenko.94@mail.ru

Received September 29, 2021; revised October 6, 2021; accepted October 7, 2021

Abstract—The method of mathematical modeling was used to determine the rate of cooling of the heat-affected zone upon assembling the weld joints of reactor plants for nuclear icebreakers by preweld depositions. The effect of thermal cycles in various sections of deposited metal welded using three types of welding consumables, namely, carbon steel, silicon-manganese steel, and steel alloyed with nickel, was simulated using a quenching deformation dilatometer. The structure and hardness of the samples after simulated exposure to thermal welding cycles were studied. The deposited metal in using a Sv-06AA carbon wire was found to have a ferrite-pearlite structure throughout the range of cooling rates. An Sv-08GS manganese silicon wire forms an acicular ferrite structure in a wide range of cooling rates, while an Sv-10GN steel wire alloyed with nickel forms an acicular and quasi-polygonal ferrite structure.

Keywords: simulation of thermal welding cycles, preweld deposition, acicular ferrite, pearlite, thermokinetic diagram

DOI: 10.1134/S2075113322060260

INTRODUCTION

In circumstances when a series of Project 22220 *Arktika* nuclear icebreakers are under extensive construction and the launch order for a Project 10510 *Leader* nuclear icebreaker has started to be executed, a performance gain upon welding of their reactor plants and an improvement in the weld quality are of current concern. The nuclear reactor pressure vessels of icebreakers are manufactured using 15Kh2MFA mod, a heat-resistant steel. Its welding features the need for preliminary and concurrent heating at 175–250°C directly followed by high-temperature tempering at $655 \pm 10^\circ\text{C}$ (intermediate) and $670 \pm 10^\circ\text{C}$ (final) (avoiding cooling below 175°C) [1]. Such a feature is due to the tendency of steel to form quenching structures having low resistance to brittle fractures.

The lack of a technical possibility to carry out high-temperature tempering because of structural features is a problem in making some weld joints of reactor plant assembly units. In this case, the emergence of quenching structures in the heat-affected zone is prevented by applying the following process: welded edges are preliminarily overlaid with low-carbon deposition by automatic submerged-arc welding using an Sv-06AA wire and AN-42M flux or by manual welding with UONII-13/55 electrodes followed by high-

temperature tempering. The weld is made using the same consumables as used in preweld deposition. The application of this process prevents the formation of quenching structures in the heat-affected zone with weld being made without subsequent tempering. However, the statistical analysis [2] of data from testing of production check welding samples in the manufacture of transport power facilities showed that, in some cases, the strength properties of such joints cannot be provided at a sufficient level.

The studies of [3] found that the metal of preweld low-carbon deposition made by automatic submerged-arc welding using an Sv-06AA wire and an AN-42M flux is substantially prone to softening on exposure to multiple high-temperature temperings unavoidable in process operations for the manufacture of reactor plant assembly units. The authors of [4] proposed the replacement of materials for preweld deposition on the basis of the test data on the properties of weld deposits built up using carbon steel, silicon manganese steel, and alloyed steel wires of different composition in combination with different-type fluxes. It was found [4] that the most optimum ratio of strength and plastic properties, hardness, and impact viscosity is provided by the Sv-08GS silicon–manganese wire

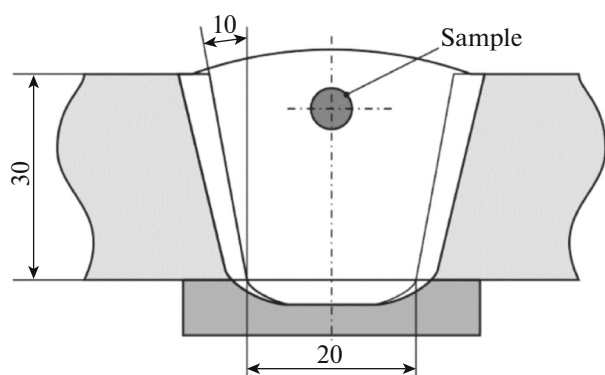


Fig. 1. Sketch of cutout of samples made of deposited weld metal.

or the Sv-10GN nickel alloy wire upon automatic submerged-arc welding under the 48AF-71 flux.

Taking into account a specific responsibility of the reactor plant equipment of under-construction and promising nuclear icebreakers, the preweld deposits of which are important structural elements, it is interesting to study the structure formation on exposure to thermal cycles of welding using the proposed consumables.

The aim of the present work was to conduct a comparative study of the structural phase transformations of preweld metal of assembling weld joints made using the earlier used consumables and their proposed substitutions.

RESEARCH PROCEDURE

The studies were carried out on deposited metal samples made by automatic submerged-arc welding using three combinations of welding consumables. The diagram of structural weld elements is shown in Fig. 1. The parent base metal was St3sp5 steel.

The materials applied in welding and the chemical composition of the weld metal according to the data of [4] are given in Table 1. The test samples appeared as cylinders with a length of 10 mm and a diameter of 5 mm. For notational convenience, the metal samples are denoted hereinafter as A, B, and C.

Sample A was cut out of a deposited metal made using a low-carbon wire and a fused silicon-manga-

nese flux containing $\approx 0.3\%$ of silicon and $\approx 1\%$ of manganese.

Sample B was cut out of a deposited metal made using a silicon manganese wire under chemically neutral ceramic flux and differs from sample A in a slightly higher ($\approx 1.3\%$) content of manganese.

Sample C differs from two previous ones mainly in the presence of nickel at a level of $\approx 1\%$.

The effect of thermal cycles during multi-pass welding on the formation of the weld metal structure was simulated using a DIL 805 high-speed quenching-deformation dilatometer (BAHR Thermoanalyse, Germany). According to the scheme recommended in [5], the samples in the dilatometer were vacuum heated by high-frequency currents, and cooling at specified rate was carried out by supply of helium.

To select the rate of metal cooling, in this study, the thermal cycles of welding over preweld depositions were computer simulated by the finite element method in the ANSYS software package [6].

Structures were studied on transverse sections using an Axio Observer 3 light inverted-stage metallographic microscope (Zeiss) forming a part of the Thixomet hardware and software system for the microstructural analysis of solid surfaces. The structure was developed by etching in 4% alcohol solution of nitric acid [7].

The hardness of sample material was measured at three points on the longitudinal cross-sectional surface by the Vickers method in accordance with GOST 2999-75 using a 5030SKV hardness meter (Zwik) at a load of 10 kgf.

RESULTS AND DISCUSSION

During simulation of thermal cycles in making a weld joint over preweld deposition, we developed a geometric model with dimensions of $700 \times 250 \times 30$ mm and division of the body into finite elements. Calculations were performed in the symmetric formulation. The symmetry plane passed perpendicularly to the deposited surface along the displacement axis of the heating source. For regions with expectedly high temperature gradients (deposited metal, weld-adjacent zone, and contemplated heat-affected zone), the finite elements were made with significantly smaller size compared to the elements in the geometrical model sections remote from the weld zone (gradient

Table 1. Chemical composition of the weld metal

Sample	Welding consumables: wire/flux	Content of chemical elements, wt %								
		C	Si	Mn	Cr	Mo	Ni	Cu	S	P
A	Sv-06AA/AN-42M	0.04	0.33	0.91	0.14	0.01	0.21	0.06	0.006	0.009
B	Sv-08GS/48AF-71	0.04	0.38	1.35	0.31	0.04	0.20	0.02	0.008	0.009
C	Sv-10GN/48AF-71	0.06	0.18	1.00	0.10	0.03	0.97	0.15	0.012	0.011

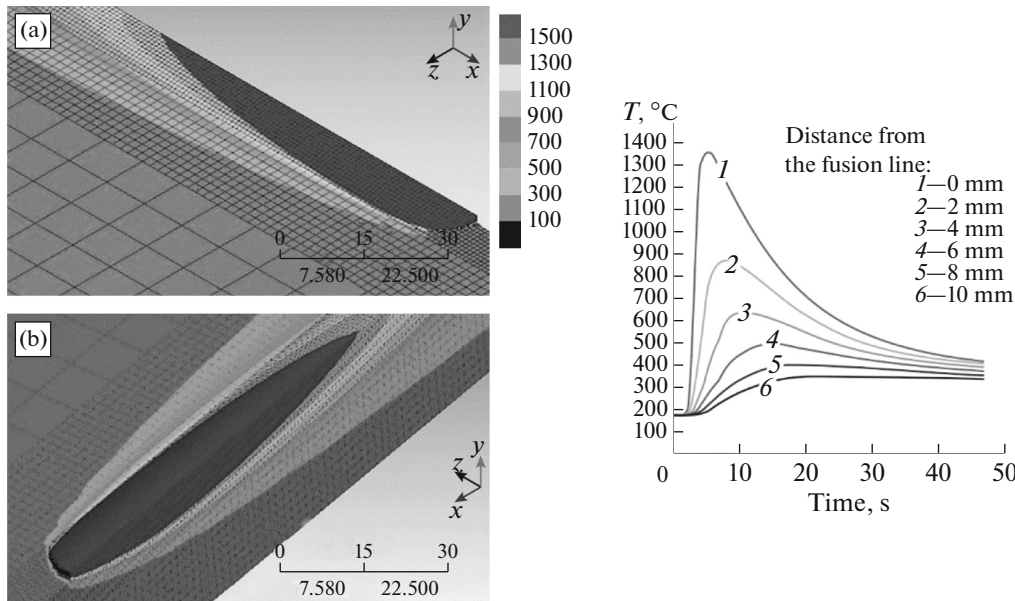


Fig. 2. Data of computer simulation for thermal processes during weld deposition: (a, b) temperature fields and (c) thermal cycles at different distance from the weld-fusion line.

mesh). This approach allows one to increase the accuracy of solution and to considerably reduce the calculation time.

Upon simulation of materials, temperature-dependent thermophysical properties were handled. The used heating source model was developed taking into account the stepwise formation of deposited weld metal as far as displacement of the welding arc. This was realized by the technology of finite element birth and death [8] using a custom-written APDL code (ANSYS Parametric Design Language). It was assumed that all heat is transmitted through the deposited metal. This procedure was verified in [9].

The boundary conditions were taken as follows:

- The parent metal was a low-alloy steel.
- The preheating temperature was 175°C.
- The conditions of weld deposition: the current was 500 A, the voltage was 32 V, and the rate was 27 m h⁻¹.
- Convection took place from free surfaces into air.

The temperature fields and plotting data for thermal welding cycles at the distance of up to 10 mm from the weld-fusion line are given in Fig. 2.

The average rate of cooling at the weld-fusion line in the temperature range between the critical points Ac_3 and Ac_1 is 14°C s⁻¹. The rate of cooling at the distance of 4 mm from the weld-fusion line (the boundary of heat-affected zone) is approximately 5°C s⁻¹. With an increase in the distance from the weld-fusion line above 4 mm, the temperature does not reach the Ac_1 line.

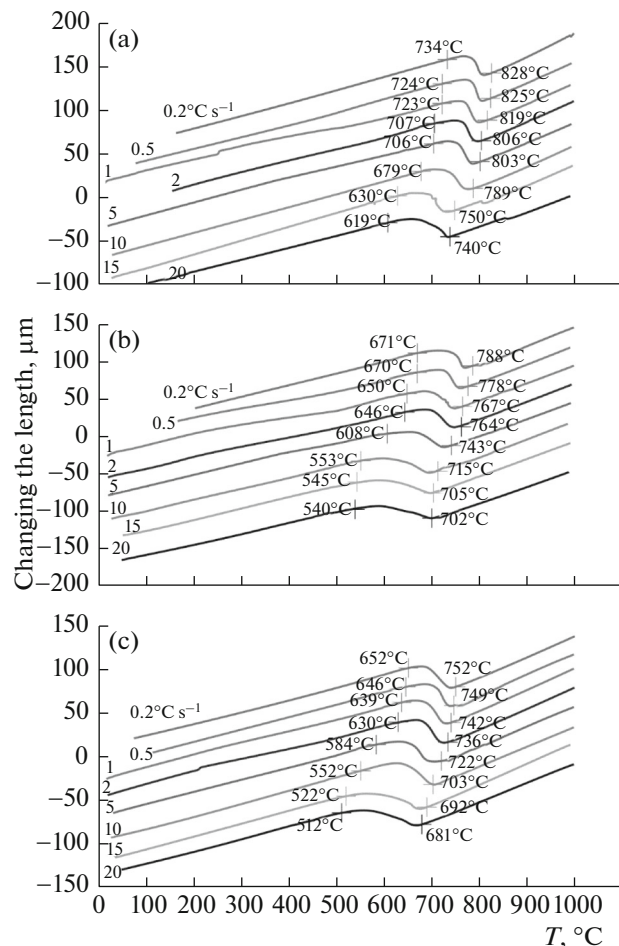


Fig. 3. Change in the length of samples A, B, and C (a, b, and c, respectively) as a function of temperature at cooling rates from 0.2 to 20°C s⁻¹.

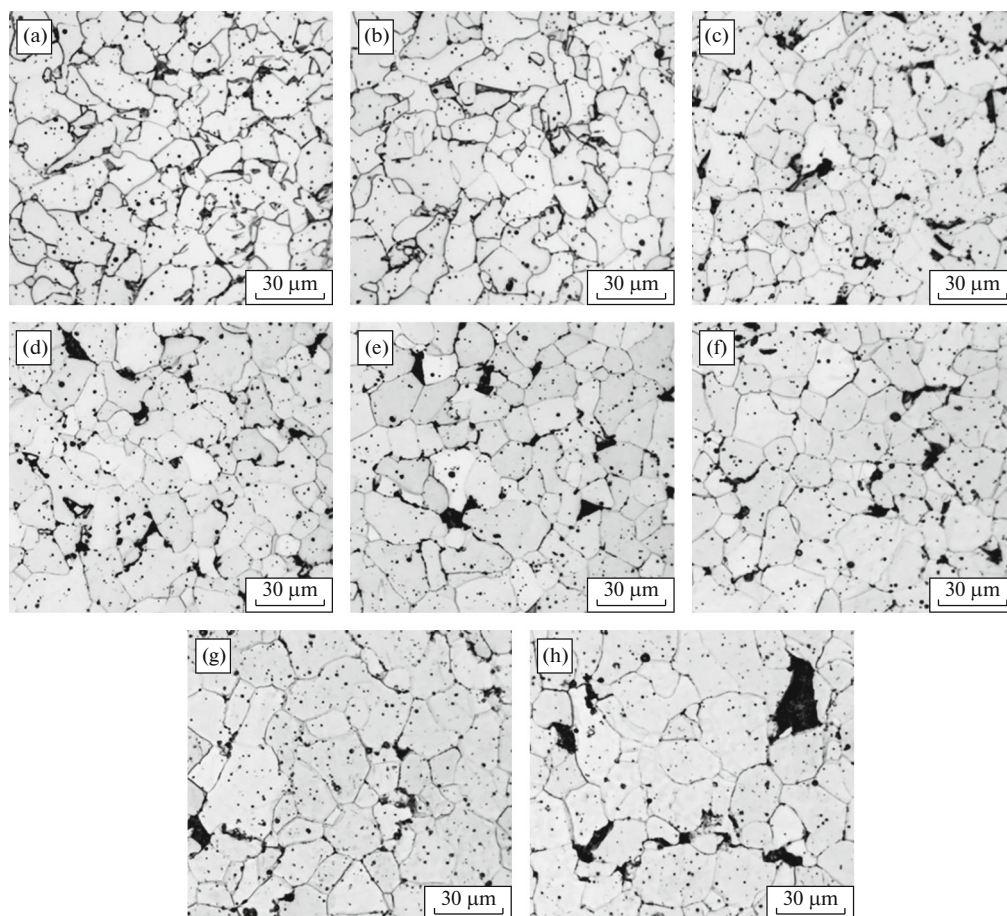


Fig. 4. Structure of the samples of material A after cooling at different rates: (a) 20° , (b) 15; (c) 10; (d) 5; (e) 2; (f) 1; (g) 0.5, and (h) $0.2^{\circ}\text{C s}^{-1}$.

Thus, the structure formation of deposited metal at a cooling rate from 5 to $15^{\circ}\text{C s}^{-1}$ is of interest.

Upon simulation of thermal cycles using the quenching and tempering dilatometer, the parameters were selected so that the cooling rate was 20, 15, 10, 5, 2, 1, 0.5, and $0.2^{\circ}\text{C s}^{-1}$. The value of $20^{\circ}\text{C s}^{-1}$ was taken as a hypothetical rate in the case of deviation from the welding procedure to a decreased preheating temperature. The values of 2, 1, 0.5, and $0.2^{\circ}\text{C s}^{-1}$ are contemplated cooling rates in case of deviation from the welding procedure to a considerable increase in the preheating temperature.

The start of phase changes upon degradation of supercooled austenite was determined by the beginning of deviation of the dilatogram from the straight-line course of the curve characterizing the linear size (length) of the sample as a function of temperature. Series of cooling curves are shown in Fig. 3.

The critical points Ac_1 and Ac_3 were determined by dilatometric studies during heating of the samples. For the materials of samples A and B, owing to the similarity of their chemical compositions, the initial points of

polymorphic (α - γ) transformation Ac_1 are close (735 and 720°C) and the final points of polymorphic (α - γ) transformation Ac_3 coincide (900°C). The presence of nickel at a level of $\approx 1\%$ in sample C (Table 1) has an effect on the displacement of the critical points: $Ac_1 = 715^{\circ}\text{C}$ and $Ac_3 = 870^{\circ}\text{C}$.

A structural change of the metal of samples A, B, and C as a function of the cooling rate is shown in Figs. 4, 5, and 6, respectively. In sample A, at a cooling rate of $20^{\circ}\text{C s}^{-1}$, the structure is represented by polygonal ferrite (the light sections in Fig. 4a) with carbide inclusions, as well as by perlite (the dark sections in Fig. 4a). At a cooling rate from 10 to $0.2^{\circ}\text{C s}^{-1}$ (Figs. 4b–4h), the percentage of the perlite component in the structure of the samples decreases with an increase in the size of perlite grains. The grain size of polygonal ferrite also increases from $\approx 20\ \mu\text{m}$ at a cooling rate of $20^{\circ}\text{C s}^{-1}$ to $\approx 50\ \mu\text{m}$ at a cooling rate of $0.2^{\circ}\text{C s}^{-1}$.

The structure of sample B at a cooling rate from 20 to $10^{\circ}\text{C s}^{-1}$ (Figs. 5a–5c) is represented by acicular ferrite. When the cooling rate was decreased to 5°C s^{-1} ,

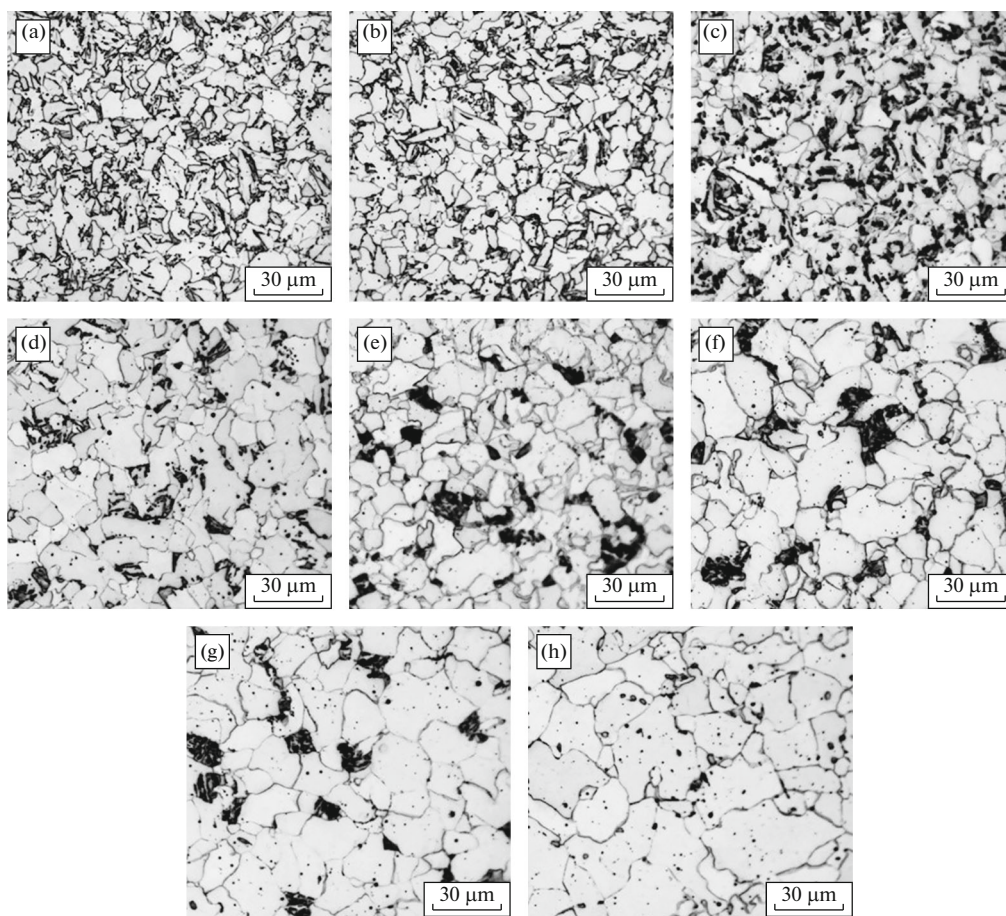


Fig. 5. Structure of the samples of material B after cooling at different rates: (a) 20, (b) 15; (c) 10; (d) 5; (e) 2; (f) 1; (g) 0.5, and (h) $0.2^{\circ}\text{C s}^{-1}$.

the percentage of acicular ferrite decreased to $\approx 30\%$ (Fig. 5d). With further decrease in the cooling rate, the structure appeared as polygonal ferrite and carbides with perlite regions similar to the material of sample A.

At cooling rates from 20 to $15^{\circ}\text{C s}^{-1}$, the structure of the material of sample C is represented by a homogeneous mixture of acicular and polygonal ferrites (Figs. 6a, 6b). Upon a decrease in the cooling rate to 5°C s^{-1} (Figs. 6c, 6d), the structure in contrast to sample B material is represented by quasi-polygonal ferrite [10] and perlite, which is likely explained by a decrease in the critical point A_{c1} . At a cooling rate less than 5°C s^{-1} , the structure like that for the materials of samples A and B is represented by a mixture of polygonal ferrite and perlite (Figs. 6e–6h). This material differs from the previous ones in the smallest grain size: the average grain size at a cooling rate of $10^{\circ}\text{C s}^{-1}$ is $\approx 15\ \mu\text{m}$ and that at a cooling rate $0.2^{\circ}\text{C s}^{-1}$ is $\approx 30\ \mu\text{m}$, which is explained by the presence of nickel in its composition.

The measured hardness of samples A, B, and C as a function of the cooling rate is shown in Fig. 7. In all

considered cases, the hardness does not exceed 190 HV units, which suggests no tendency to form quenching structures upon welding with selected consumables.

At cooling rates of 20 – $10^{\circ}\text{C s}^{-1}$, the hardness of samples B and C was 160–180 HV units, which corresponded to that of acicular ferrite, and the hardness of sample A was ≈ 150 HV units and remained unchanged until the cooling rate of $0.5^{\circ}\text{C s}^{-1}$. When the cooling rate was decreased to $0.5^{\circ}\text{C s}^{-1}$, samples B and C exhibited a gradual decrease in the hardness, which is explained by the predominance of the polygonal ferrite percentage over the acicular one up to the values for sample A. At a cooling rate of $0.2^{\circ}\text{C s}^{-1}$, the hardness decreased for all three samples to 130–140 HV units.

The thermal kinetic diagrams of austenite transformation given in Fig. 8 for the material of samples A, B, and C were plotted according to the data of dilatometric (Fig. 3) and metallographic (Figs. 4–6) studies and hardness measurements (Fig. 7).

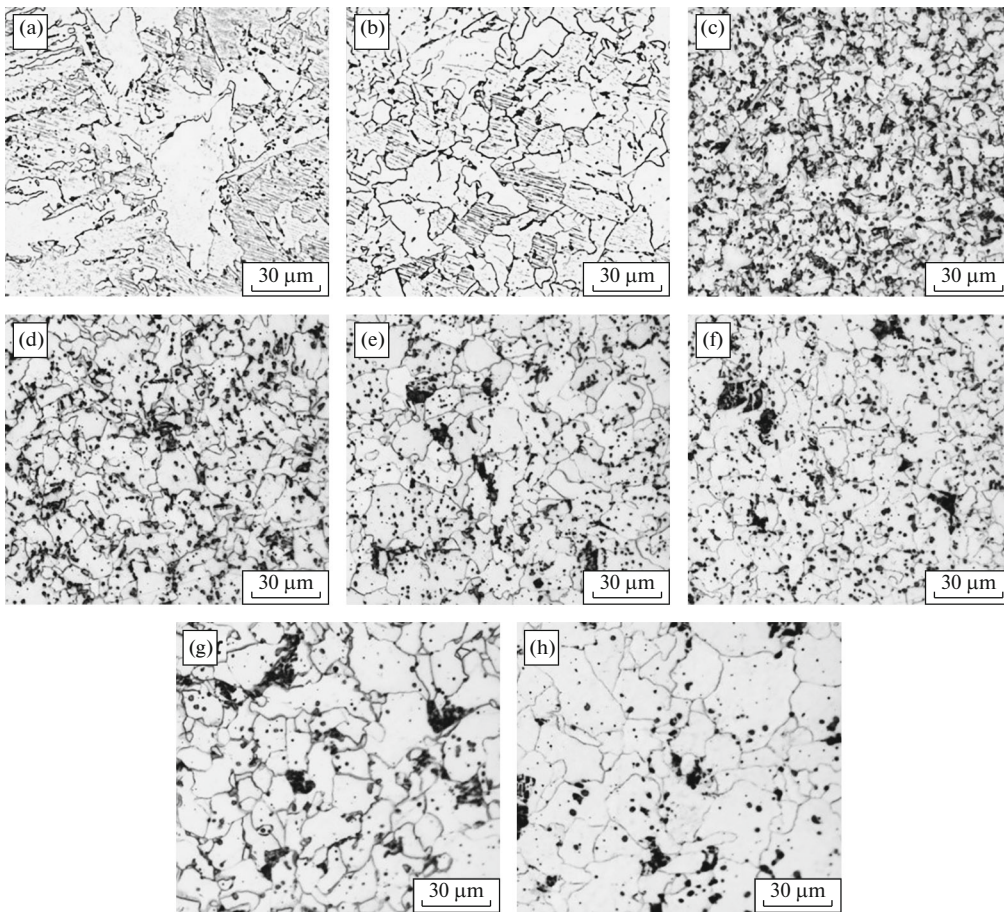


Fig. 6. Structure of the samples of material C after cooling at different rates: (a) 20, (b) 15; (c) 10; (d) 5; (e) 2; (f) 1; (g) 0.5, and (h) $0.2^{\circ}\text{C s}^{-1}$.

Analyzing the obtained data, one should note that the material of sample A (metal deposited using the Sv-06AA weld wire under the AN-42M flux) throughout the range of cooling rates has a polygonal ferrite structure with regions of perlite and carbides. Such a structure is due to the chemical composition (the lowest total content of alloying silicon and manganese

additives). Thus, the data of [2, 3] are confirmed, suggesting that the strength of preweld low-carbon metal of reactor plants cannot be increased using engineering measures during welding.

The material of sample B (metal deposited using the Sv-08GS wire under the 48AF-71 flux) containing a slightly higher total amount of silicon and manganese at real cooling rates from 14 to 5°C s^{-1} , as determined by calculation, provides the structure of acicular ferrite being the most favorable in terms of the combination of strength and plastic characteristics and in terms of the brittle fracture resistance. In this case, the material is not prone to the formation of quenching structures even if the cooling rate upward deviates from the real conditions.

The material of sample C (metal deposited using the Sv-10GN wire under the 48AF-71 flux) had an acicular ferrite structure at cooling rates from 20 to $10^{\circ}\text{C s}^{-1}$ and a quasi-polygonal ferrite structure with lower hardness than that for the material of sample B when the cooling rate was decreased to 5°C s^{-1} .

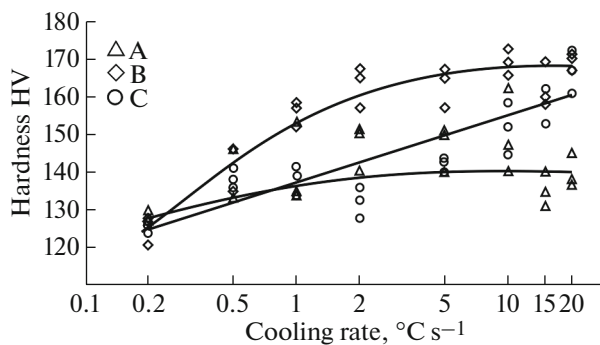


Fig. 7. Hardness as a function of the cooling rate.

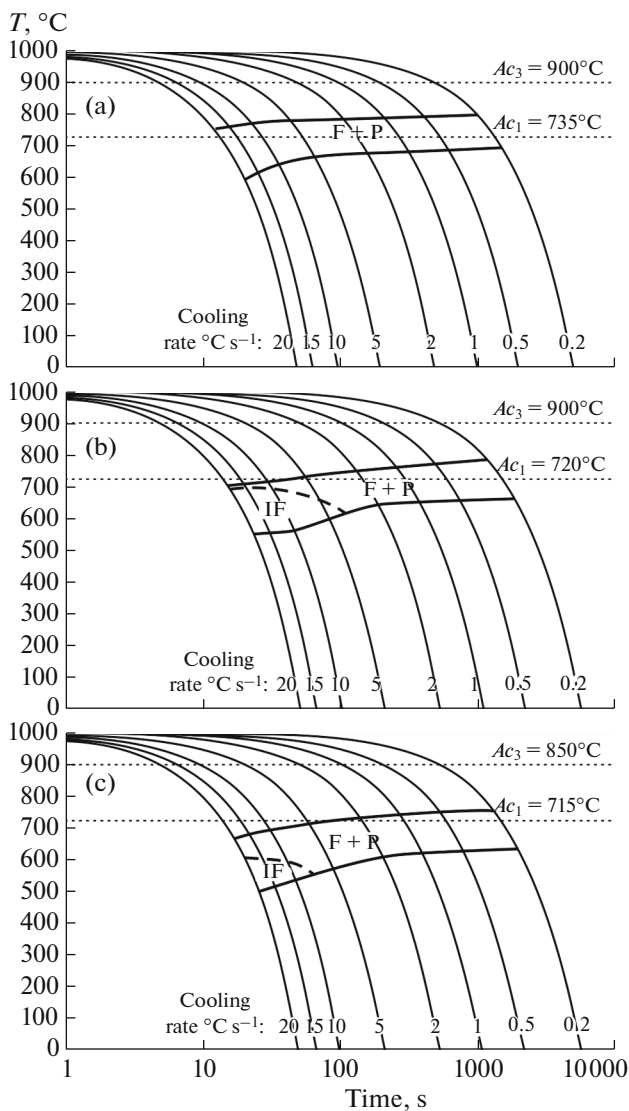


Fig. 8. Thermal kinetic diagram of austenite transformation in the material of samples A, B, and C (a, b, and c, respectively).

Thus, the material of sample C is structurally more susceptible to overheating than that of sample B upon exceeding the welding speed and the temperature of preliminary and concurrent heating.

Thus, the study of the structural phase transformations in the metal welded using the studied consumables found that the application of the Sv-08GS weld wire and 48AF-71 flux (material of sample B) upon automatic submerged-arc welding is the most favorable combination in terms of providing the required characteristics of power supply units in nuclear icebreakers.

CONCLUSIONS

The range of cooling rates under conditions of welding over preweld deposition on the edges of

assembly units for reactor plant equipment of nuclear icebreakers was determined by the calculation method. At temperatures from Ac_3 to Ac_1 , the average cooling rate is from 14 to 5°C s^{-1} depending on the distance of the preweld overlay region from the weld-fusion line.

The structural formation features of preweld metal made with three types of consumables for automatic welding were revealed under conditions of cooling at rates from 0.2 to 20°C s^{-1} . The structure of metal overlaid using the Sv-06AA wire under the AN-42M flux at cooling rates from 0.5 to 20°C s^{-1} appeared as a polygonal ferrite with perlite inclusions. The structure of metal overlaid using the Sv-80GS and Sv-10GN wire under the 48AF-71 flux at cooling rates from 10 to 20°C s^{-1} was represented by acicular ferrite. When the cooling rate of the metal welded with Sv-08GS wire was decreased to 0.5°C s^{-1} , the acicular ferrite smoothly transformed to polygonal ferrite, whereas the structure of the metal welded with Sv-10GN wire dramatically transformed to quasipolygonal ferrite characterized by a decreased hardness. At a cooling rate of 0.2°C s^{-1} , the structure for all studied versions was represented by polygonal ferrite with perlite grain inclusions characterized by a hardness of ≈ 130 –140 HV units.

It was found that none of the considered consumables were prone to the formation of quenching structures under automatic welding conditions.

The thermal kinetic diagrams of austenite transformation were plotted for the studied materials on the basis of the dilatometric and metallographic studies and the hardness measurements. The use of the Sv-08GS welding wire and the 48AF-71 flux provided an acicular ferrite structure and hardness of 160–180 HV units in the real temperature range and was found to be the most favorable combination in terms of achieving the required characteristics of assembling weld joints of power plants in nuclear icebreakers.

FUNDING

Experimental studies were performed using equipment of the Center for Collective Use Composition, Structure, and Properties of Structural and Functional Materials at the National Research Center Kurchatov Institute—CRISM Prometey with financial support from the Ministry of Science and Higher Education of the Russian Federation (agreement no. 13.TsKP.21.0014 (075-11-2021-068), unique identifier RF-2296.61321X0014).

CONFLICT OF INTEREST

The authors declare that they have no conflicts of interest.

REFERENCES

1. *Federal'nye normy i pravila v oblasti ispol'zovaniya atomnoi energii. Svarka i naplavka oborudovaniya i truboprovodov atomnykh energeticheskikh ustanovok (NP-104-18)* (Federal Norms and Rules in the Field of the Atomic Energy Use. Welding and Surfacing of Equipment and Pipelines of Nuclear Power Plants (NP-104-18)), Moscow: Fed. Sluzhba Ekol., Tekhnol. At. Nadzoru, 2018.
2. Timofeev, M.N., Karzov, G.P., Galiatkin, S.N., Mikhaleva, E.I., Litvinov, S.G., Aleksandrin, A.G., Bashulin, D.L., and Shubin, O.V., Improvement of the service properties of the weld joint metal for transport nuclear power units manufactured of heat-resistant steel grades: Part I. Technology of welding heat-resistant steel grades using low-carbon welding materials without heat treatment and experience of applying welding materials, *Inorg. Mater.: Appl. Res.*, 2018, vol. 9, pp. 1142–1147. <https://doi.org/10.1134/S2075113318060242>
3. Timofeev, M.N., Galiatkin, S.N., Mikhaleva, E.I., and Shubin, O.V., Improvement of the service properties of the weld joint metal for transport nuclear power units manufactured of heat-resistant steel grades: Part II. A study of mechanical properties of low-carbon weld deposits depending on the welding process variables, *Inorg. Mater.: Appl. Res.*, 2018, vol. 9, pp. 1148–1154. <https://doi.org/10.1134/S2075113318060254>
4. Timofeev, M.N., Galiatkin, S.N., and Mikhaleva, E.I., Improvement of the service properties of the weld joint metal for transport nuclear power units manufactured of heat-resistant steel grades: Part III. A study of the influence of alloying elements on the characteristics of the all-weld metal as applied to the fabrication of low-carbon metal deposits and assembly weld joints in ice-breaker nuclear power units, *Inorg. Mater.: Appl. Res.*, 2018, vol. 9, pp. 1155–1164. <https://doi.org/10.1134/S2075113318060266>
5. Barakhtin, B.K. and Nemets, A.M., *Metally i splavy. Analiz i issledovanie. Fiziko-analiticheskie metody issledovaniya metallov i splavov. Nemetallicheskie vklyucheniya: Spravochnik* (Metals and Alloys. Analysis and Research. Physico-Analytical Methods for the Metals and Alloys Study. Nonmetal Inclusions: Handbook), St. Petersburg: Professional, 2006.
6. ANSYS Software Package. <http://www.ansys.com>. Accessed September 12, 2021.
7. Brandon, D. and Kalan, W.D., *Microstructural Characterization of Materials*, Chichester: Wiley, 1999.
8. Kuznetsov, V.V., Vodiakov, V.N., and Kuznetsova, O.M., Technology of birth and death of finite elements of ANSYS Inc. (USA), in *Energoeffektivnye i resursoberegayushchie tekhnologii i sistemy* (Energy-Efficient and Resource-Saving Technologies and Systems), Kotin, A.V. et al., Eds., Saransk: Mordovsk. Univ., 2013, pp. 392–401.
9. Korolev, S.A. and Zimakov, A.E., Computer simulation of thermal processes in arc welding of thick-walled aluminum alloy structures, *Izv. Vyssh. Uchebn. Zaved., Mashinost.*, 2020, no. 8, pp. 12–20.
10. Matrosov, M.Yu., Lyasotskii, I.V., Kichkina, A.A., et al., Microstructure in low-carbon low-alloy high-strength pipe steel, *Steel Transl.*, 2012, vol. 42, pp. 84–93. <https://doi.org/10.3103/S0967091212010135>
11. Lebedeva, N.V., Markova, Yu.M., Ziza, A.I., and Anisimov, D.M., Study of the microstructure of martensite-bainite steels and nickel alloys when modeling heat treatment modes using a dilatometric method, *Zavod. Lab. Diagn. Mater.*, 2019, vol. 85, no. 6, pp. 30–36. <https://doi.org/10.26896/1028-6861-2019-85-6-30-36>

Translated by K. Utegenov